Research Square

Preprints are preliminary reports that have not undergone peer review.
They should not be considered conclusive, used to inform clinical practice,
or referenced by the media as validated information.

Comparison of the Diagnostic Performance of Different Coronary Functional Assessment Methods in Moderate-to-Severe Stenosis: A Real-World Study

Li Huang
The Affiliated LiHuiLi Hospital of Ningbo University
Mingjie Wu
The Affiliated LiHuiLi Hospital of Ningbo University
Xiao Xu
The Affiliated LiHuiLi Hospital of Ningbo University
Yuqin Zhang
zyqlucky168@163.com

The Affiliated LiHuiLi Hospital of Ningbo University

Research Article

Keywords: Coronary computed tomography angiography, Coronary stenosis, Diagnostic performance, Functional ischemia, Fractional flow reserve, Quantitative flow ratio.

Posted Date: November 18th, 2026

DOI: https://doi.org/10.21203/rs.3.rs-11297238/v1

License: This work is licensed under a Creative Commons Attribution 4.0 International License.
Read Full License

Additional Declarations: No competing interests reported.

Abstract

Background

Clinical management of moderate-to-severe coronary stenosis depends substantially on whether a lesion causes functional ischemia. Although invasive fractional flow reserve (FFR) serves as the reference standard for functional evaluation, its routine application is constrained by procedural invasiveness, examination time, drug tolerance, and resource requirements. By deriving CT-FFR from coronary computed tomography angiography (CCTA) and obtaining Murray law-based quantitative flow ratio (μQFR) from invasive coronary angiography (ICA), less invasive and more efficient functional assessment approaches become achievable. However, direct comparisons of different CT-FFR algorithms with ICA-based μQFR remain scarce for lesions with 50%–90% stenosis, especially when domestically developed CT-FFR software based on distinct computational techniques is considered.

Methods

Patients undergoing CCTA, ICA, and FFR measurement within a 30-day interval from January 2018 through December 2025 were retrospectively screened. After applying the predefined inclusion and exclusion criteria, 49 patients with 51 target vessels exhibiting visually assessed moderate-to-severe coronary stenosis (50%–90%) were ultimately enrolled. Using FFR as the benchmark, two CT-FFR algorithms and μQFR underwent evaluation and comparison for diagnostic performance.

Results

The two CT-FFR algorithms and μQFR were successfully evaluated in all 51 vessels. For CT-FFR1, sensitivity, specificity, and accuracy were 80.95% [95% confidence interval (CI), 58.09%–84.55%], 66.67% (95%CI, 47.19%–82.71%), and 72.55% (95%CI, 58.26%–84.11%), respectively. The corresponding values for CT-FFR2 were 61.91% (95%CI, 38.44%–81.89%), 83.33% (95%CI, 65.28%–94.36%), and 74.51% (95%CI, 60.37%–85.67%), while those for μQFR were 76.19% (95%CI, 52.83%–91.78%), 83.33% (95%CI, 65.28%–94.36%), and 80.39% (95%CI, 66.89%–90.18%), respectively. The area under the receiver operating characteristic curve (AUC) reached 0.73 (95%CI, 0.58–0.88) for CT-FFR1, 0.73 (95%CI, 0.60–0.87) for CT-FFR2, and 0.81 (95%CI, 0.69–0.94) for μQFR. None of the pairwise comparisons among the three methods reached statistical significance (all $P > 0.05$).

Conclusions

Each of the three imaging-derived functional assessment methods demonstrated diagnostic capability for detecting functional ischemia in moderate-to-severe coronary lesions (50%–90%). μQFR yielded the highest AUC and accuracy while maintaining relatively balanced sensitivity and specificity. The two CT-

FFR software demonstrated similar overall diagnostic performance, although their individual diagnostic indices differed. Further validation in larger, multicenter prospective studies is needed.

Trial registration

Registration number: MR-33-24-025985 Date of registration: 16 April 2024

Background

Invasive coronary angiography (ICA) remains the benchmark diagnostic approach used to localize coronary lesions and determine stenosis severity among coronary artery disease (CAD) patients presenting with typical angina symptoms. According to current guidelines[1], decisions regarding revascularization should not be based exclusively on anatomical stenosis but should incorporate functional evaluation into the diagnostic and therapeutic process. During ICA, fractional flow reserve (FFR) is determined and functions as the reference standard for functional assessment. FFR is determined from the pressure gradient across a stenotic lesion using a pressure wire after sufficient microvascular vasodilation is induced with agents such as adenosine[2, 3]. However, its broader clinical use is restricted by procedural invasiveness, examination time, drug tolerance, and resource requirements. Therefore, noninvasive coronary functional assessment provides safer and more economical alternatives for evaluating whether coronary lesions are functionally significant. Common techniques comprise coronary computed tomography angiography (CCTA)-derived fractional flow reserve (CT-FFR) and Murray law-based quantitative flow ratio (μQFR), both of which are generated through quantitative analysis of existing CCTA or ICA images. A cut-off value of 0.80 is used for both indices[4, 5]. Values ≤ 0.80 indicate hemodynamically significant coronary lesions and provide functional evidence to support subsequent treatment decisions.

Previous studies primarily evaluated coronary lesions with 30%–90% stenosis and reported favorable diagnostic performance in both core laboratory off-line analyses and intraprocedural on-site QFR assessments[6–10]. Nevertheless, diagnostic accuracy may be overestimated when cohorts include vessel segments with either severe stenosis or only mild obstruction. Therefore, the applicability of these results to moderate-to-severe lesions commonly encountered in clinical practice requires further confirmation. Moderate-to-severe lesions often exhibit complex morphology and clinically significant symptoms and frequently require timely guidance regarding revascularization. Therefore, these lesions constitute an important clinical target for imaging-derived coronary functional assessment methods. Because CT-FFR and μQFR are based on different technical approaches, their diagnostic performance in the functional evaluation of moderate-to-severe lesions may not be equivalent. In this study, CCTA and ICA images obtained from the same cohort of CAD patients with typical angina symptoms were analyzed to derive three functional indices: RuiXin-FFR based on computational fluid dynamics (CFD), Dr. Wise FFR based on a deep learning model, and μQFR based on Murray's law. Utilizing FFR as the

reference standard, diagnostic performance among these three imaging-derived coronary functional assessment methods was compared for moderate-to-severe lesions.

Methods

This study adopted a retrospective cohort design, conducted at the Affiliated LiHuiLi Hospital of Ningbo University.

Study Population and Inclusion and Exclusion Criteria

Patients admitted to the Affiliated LiHuiLi Hospital of Ningbo University from January 2018 to December 2025 were eligible if: (1) visual assessment of CCTA identified at least one moderate-to-severe stenotic lesion in a major epicardial coronary artery; (2) Within 30 days of clinical indication, ICA and FFR measurements were subsequently performed. Per CAD-RADS 2.0[11], lesions with 50%–69% stenosis are categorized as moderate stenosis (CAD-RADS 3), whereas lesions with 70%–99% stenosis are categorized as severe stenosis (CAD-RADS 4A). Lesions with stenosis > 90% are further classified by CAD-RADS 2.0 as a high-risk subgroup of severe stenosis. In such cases, direct invasive coronary angiography is preferred for clinical evaluation and treatment planning, and CT-FFR analysis is not recommended. Therefore, moderate-to-severe stenosis in this study was defined specifically as 50%–90% stenosis.

CT-FFR analysis excluded patients meeting any of the following criteria: (1) inadequate CCTA image quality, defined as an image quality rating below “good”; (2) documented New York Heart Association functional class III or higher, or a history of coronary artery bypass grafting, prosthetic heart valve implantation, pacemaker or implantable cardioverter-defibrillator implantation, or hypertrophic obstructive cardiomyopathy; (3) myocardial bridging or a previously implanted metallic stent in the interrogated vessel; or (4) collateral circulation detected on ICA. Exclusion criteria for μQFR analysis were as follows: (1) marked overlap of the interrogated vessel on coronary angiography; (2) inadequate ICA image quality; or (3) severe vessel tortuosity on coronary angiography that impaired accurate lumen reconstruction.

The vessel served as the unit of analysis. In patients with multiple diseased vessels satisfying the inclusion criteria, every target vessel subjected to invasive FFR measurement was included. A total of 67 patients who underwent both CCTA and ICA with FFR measurement were initially screened for eligibility. Then 7 patients were excluded: 2 because the interval between CCTA and invasive FFR exceeded 30 days, 2 because the original CCTA and/or ICA images were missing, and 3 because they were in New York Heart Association functional class III or higher. The remaining 60 consecutive patients contributed a total of 65 target vessels. Of these, 14 vessels were further excluded: 6 because of myocardial bridging in the target vessel, 1 because of prior PCI in the target vessel, 6 because of poor image quality (3 due to image noise and 3 due to beam-hardening artifacts), and 1 because of CCTA import failure for CT-FFR analysis. Finally, 49 patients with 51 target vessels were included in the analysis. Baseline

characteristics were recorded at the patient level. For patients with more than one eligible vessel, baseline data were duplicated according to the number of diseased vessels.

CCTA Acquisition and Post-processing

CCTA procedures adhered to the guidelines established by the Society of Cardiovascular Computed Tomography[12]. A 256-slice CT system (Revolution CT, GE Healthcare, USA) was employed to perform all examinations. Before scanning, patients fasted and avoided water intake for 4–6 h and received breathing training. Heart rate was maintained below 70 beats/min, and scanning was conducted with patients in the supine, head-first position. A prospective electrocardiographically gated cardiac acquisition protocol was applied. Scanning parameters were set as follows: a 0.625 mm × 256 collimator width, 0.625 mm reconstruction slice thickness and interval, 0.28 s gantry rotation time, 100 kV tube voltage, 300–500 mAs tube current, along with intelligent sector selection scanning mode. Iohexol (350 mg I/mL) served as the contrast medium and was administered through an antecubital vein with a high-pressure injector (Ulrich, Germany) at 5–5.5 mL/s, using a total volume of 55–65 mL. Subsequently, a 30-mL saline flush was administered at an identical rate. An automatic bolus-tracking method was applied, with the trigger level positioned at the ascending aortic root, the region of interest placed within the ascending aorta, and the trigger threshold set at 250 Hounsfield units (HU). The scan extended from the tracheal carina to 20 mm below the diaphragm, thereby covering the aortic root, the entire coronary arteries, and the cardiac apex. The total scanning time was 0.4 s. After image acquisition, all data were transferred to a post-processing workstation.

CCTA raw data were reconstructed with the standard cardiac reconstruction algorithm, and either the 75% or 45% phase was selected for post-processing according to the software prompts. Stenosis severity was computed according to the formula: (normal vessel diameter proximal to the stenotic lesion − diameter at the stenosis) / proximal normal vessel diameter × 100%.

ICA and Invasive FFR Measurement

ICA was conducted based on relevant clinical guidelines[13], with the indication determined by integrated consideration of patient symptoms, response to medical therapy, CCTA findings, and noninvasive functional test results. The procedure followed established standards, and each major epicardial coronary artery was imaged from multiple projections. Stenosis severity was visually evaluated by experienced cardiologists. Invasive FFR measurement was conducted according to guideline recommendations[2]. Before advancement into the coronary artery, the pressure wire was zeroed, followed by equalization of aortic (Pa) and distal coronary (Pd) pressures at the catheter tip. Subsequently, the pressure wire was advanced beyond the target lesion, with its tip placed distal to the stenotic segment. Maximal hyperemia was induced via continuous intravenous adenosine infusion, with the FFR value defined as the minimum Pd/Pa ratio observed throughout the stable hyperemic period. Pressure drift was assessed after each measurement, and measurements were repeated when the drift

exceeded the predefined threshold. According to the guidelines[1, 14], functional ischemia was defined as FFR ≤ 0.80, while FFR values of 0.70–0.80 were classified as the gray zone.

Imaging-Derived Coronary Functional Assessment

To ensure consistency between the measurement locations used for imaging-derived coronary functional assessment and invasive FFR, an independent investigator with 7 years of experience in coronary angiography interpretation identified and documented the target lesion sites evaluated by invasive FFR from the ICA procedural records. CT-FFR and μQFR analyses were independently conducted by two experienced radiologists, all of whom completed standardized training before analysis. Throughout the measurement process, operators were kept unaware of one another's findings as well as the invasive FFR values, with the exception of the target lesion location. For CT-FFR, measurements were obtained 2 cm distal to the target lesion[15, 16]. Because previous studies found no significant difference between μQFR measured 2 cm distal to the lesion and μQFR measured at the distal end of the target vessel[17], only the value at the distal end of the target vessel was obtained for μQFR.

CT-FFR analysis was performed on CCTA images using two software platforms: RuiXin-FFR (V2.0, Shenzhen Raysight Intelligent Medical Technology Co., Ltd, Shenzhen, Guangdong, China) and Dr. Wise FFR (V1.0, Hangzhou Deepwise & League of PHD Technology Co., Ltd, Hangzhou, Zhejiang, China.). Both software packages automatically generated three-dimensional reconstructions of the coronary artery tree, with manual correction of the vessel model permitted when necessary. RuiXin-FFR used a CFD simulation approach in which individualized boundary conditions were established and hemodynamic equations were solved to derive CT-FFR. In contrast, Dr. Wise FFR applied a deep learning prediction model to directly estimate CT-FFR from coronary anatomical features. Hereafter, RuiXin-FFR and Dr. Wise FFR are referred to as CT-FFR1 and CT-FFR2, respectively. Sixty days after the initial analysis, all enrolled cases were re-measured by the same observer.

Based on ICA images, μQFR was calculated utilizing the dedicated software AngioPlus Core (V2.0, Shanghai Pulse Medical Technology Co., Ltd.). To ensure rapid and accurate μQFR calculation, an angiographic projection minimizing overlap between the target vessel and its branch ostia was selected. The major artery and its branches underwent automatic contour detection and delineation via the software. Contrast flow velocity was obtained by dividing centerline length by the filling time of the contrast medium within the artery. A pressure-drop reference diameter function was then generated according to Murray's bifurcation fractal law, from which the final μQFR value was derived. CT-FFR and μQFR values ≤ 0.80 were considered indicative of significant functional ischemia in the target vessel.

Primary Endpoint

The primary endpoint was to compare the diagnostic performance of different CT-FFR algorithms and ICA-based μQFR in identifying coronary functional ischemia in moderate-to-severe stenotic lesions.

Statistical Analysis

The Shapiro–Wilk test was employed to determine whether continuous variables followed a normal distribution. Categorical variables were denoted as frequencies and percentages; normally distributed continuous variables were denoted as mean ± standard deviation, and non-normally distributed ones as median (interquartile range). Three imaging-derived coronary functional assessment methods underwent vessel-level diagnostic evaluation, with invasive FFR employed as the reference standard. Sensitivity, specificity, accuracy, positive predictive value, negative predictive value, and 95% confidence intervals (CIs) were computed for each method, and receiver operating characteristic (ROC) analysis, including the area under the curve (AUC), was conducted to assess each method's ability to detect FFR ≤ 0.80. Spearman correlation analysis and Bland–Altman analysis were performed to assess the correlation and agreement, respectively, between each method and invasive FFR across all lesions. Intraclass correlation coefficient (ICC) analysis was conducted using data from 29 randomly selected cases. Statistical analyses were conducted with SPSS version 27.0.1.0 (IBM Corp., Armonk, NY, USA) and MedCalc version 23.4.4 (MedCalc Software, Mariakerke, Belgium).

Results

Baseline Data and Diseased Vessel Characteristics

Fifty-one baseline data records satisfying the inclusion and exclusion criteria were incorporated into the analysis(Fig. 1).

n denotes the number of vessels. CCTA, coronary computed tomography angiography; ICA, invasive coronary angiography; FFR, fractional flow reserve; CT-FFR, quantitative flow ratio derived from computed tomography angiography; μQFR indicates Murray law–based quantitative flow ratio; PCI, percutaneous coronary intervention.

Mean patient age was 64.90 ± 10.78 years. Of the 51 patients, 37 (72.50%) were male, 29 (56.90%) had hypertension, 14 (27.50%) had hyperlipidemia, and 16 (31.40%) had diabetes mellitus (Table 1).

A total of 51 diseased vessels were analyzed. Among these vessels, 35 (68.63%) were located in the left anterior descending artery (LAD), 7 (13.73%) in the left circumflex artery (LCX), and 9 (17.64%) in the right coronary artery (RCA). Stenosis of 50%–69% was observed in 13 vessels (25.49%), whereas 38 vessels (74.51%) had stenosis of 70%–90%. Invasive FFR ≤ 0.80 was identified in 21 vessels (41.18%) (Table 1).

Table 1
Baseline demographic characteristics.

Baseline characteristics of patients	**N = 51**
Age(years)	64.90 ± 10.78
Male[n(%)]	37(72.50)
Female[n(%)]	14(27.50)
Hypertension[n(%)]	29(56.90)
Diabetes mellitus[n(%)]	16(31.40)
Hyperlipidemia[n(%)]	14(27.50)
Baseline characteristics of vessels	N = 51
Target vessels	
Left anterior descending artery	35(68.63)
Left circumflex artery	7(13.73)
Right coronary artery	9(17.64)
CCTA diameter stenosis[n(%)]	
50%–69%[n(%)]	13(25.49)
70%–90%[n(%)]	38(74.51)
FFR analysis	
Vessels with invasive FFR ≤ 0.80[n(%)]	21(41.18)
Vessels with CT-FFR1 ≤ 0.80[n(%)]	27(52.94)
Vessels with CT-FFR2 ≤ 0.80[n(%)]	18(35.29)
Vessels with μQFR ≤ 0.80[n(%)]	21(41.17)

Data are denoted as mean ± SD, n (%), or median (interquartile range), as appropriate.N denotes the number of vessels. CCTA, coronary computed tomography angiography; FFR, fractional flow reserve; CT-FFR, quantitative flow ratio derived from computed tomography angiography; μQFR indicates Murray law–based quantitative flow ratio.

The distributions of CT-FFR1, CT-FFR2, and μQFR values were non-normal. Their median values were 0.80 (0.72, 0.83), 0.85 (0.75, 0.90), and 0.84 (0.73, 0.89), respectively (Fig. 2). In contrast, FFR values followed a normal distribution, with a mean of 0.82 ± 0.07.

Diagnostic Performance of the Three Imaging-Derived Coronary Functional Assessment Methods

For identifying invasive FFR ≤ 0.80, CT-FFR1 achieved an accuracy of 72.55%, a sensitivity of 80.95%, a specificity of 66.67%, a positive predictive value of 62.96%, and a negative predictive value of 83.33%. The corresponding values for CT-FFR2 were 74.51%, 61.91%, 83.33%, 72.22%, and 75.76%, respectively, while those for μQFR were 80.39%, 76.19%, 83.33%, 76.19%, and 83.33%, respectively (Table 2).

Table 2
Diagnostic performance of CT-FFR1, CT-FFR2, and μQFR.

Measure	CT-FFR1	CT-FFR2	μQFR
AUC (95% CI)	0.73(0.58–0.88)	0.73(0.60–0.87)	0.81(0.69–0.94)
Sensitivity(%)	80.95(58.09–84.55)	61.91(38.44–81.89)	76.19(52.83–91.78)
Specificity(%)	66.67(47.19–82.71)	83.33(65.28–94.36)	83.33(65.28–94.36)
Accuracy(%)	72.55(58.26–84.11)	74.51(60.37–85.67)	80.39(66.89–90.18)
PPV(%)	62.96(49.59–74.60)	72.22(52.20–86.10)	76.19(58.13–88.06)
NPV(%)	83.33(66.64–92.60)	75.76(63.90–84.65)	83.33(69.59–91.62)

μQFR indicates Murray law-based quantitative flow ratio; AUC, area under the curve; CT-FFR, quantitative flow ratio derived from computed tomography angiography; NPV, negative predictive value; PPV, positive predictive value.

For lesion-specific ischemia, μQFR yielded an AUC of 0.81 (95%CI, 0.69–0.94; $P < 0.05$), compared with 0.73 for CT-FFR1 (95%CI, 0.58–0.88; $P < 0.05$) and 0.73 for CT-FFR2 (95%CI, 0.60–0.87; $P < 0.05$) (Table 2). Taking invasive FFR as the reference standard, ROC curves were separately generated for CT-FFR1, CT-FFR2, and μQFR (Fig. 3). Pairwise ROC curve comparisons were conducted with the DeLong test. Moreover, no statistically significant differences in AUC were detected between CT-FFR1 and CT-FFR2 ($P = 0.97$), CT-FFR1 and μQFR ($P = 0.41$), or CT-FFR2 and μQFR ($P = 0.33$).

Correlation and Agreement Analyses

The distributions of CT-FFR1, CT-FFR2, and μQFR values were non-normal. Spearman correlation analysis demonstrated moderate positive associations between invasive FFR and each imaging-derived method (CT-FFR1: r = 0.411, $P = 0.003$; CT-FFR2: r = 0.438, $P = 0.001$; μQFR: r = 0.504, $P < 0.001$) (Fig. 4A, Fig. 5A, Fig. 6A).

The Bland–Altman model was selected according to the distribution of differences between invasive FFR and each imaging-derived measurement. For CT-FFR1, the mean difference from invasive FFR was 0.064 (95%CI, 0.034–0.094), with 95% limits of agreement (LoA) spanning from − 0.145 to 0.273,

suggesting that CT-FFR1 systematically underestimated invasive FFR (Fig. 4B). For μQFR, the mean difference from invasive FFR was 0.031 (95%CI, − 0.001–0.062), with 95%LoA ranging from − 0.191 to 0.252 (Fig. 6B). For CT-FFR2, the median difference from invasive FFR was 0.020 (95%CI, − 0.040–0.040), with 95%LoA ranging from − 0.155 to 0.267 (Fig. 5B). Overall, all three methods demonstrated moderate agreement with invasive FFR.

Reproducibility Analysis

To evaluate interobserver reliability, ICCs were calculated by applying a two-way random-effects model under an absolute agreement criterion. The ICC (2,1) was 0.87 (95%CI, 0.75–0.94) for CT-FFR1 and 0.86 (95%CI, 0.73–0.93) for CT-FFR2, demonstrating good agreement between observers. Test–retest reliability for a single observer was examined with a two-way mixed-effects model. The corresponding ICC (3,1) values were 0.65 (95%CI, 0.37–0.82) for CT-FFR1 and 0.65 (95%CI, 0.38–0.82) for CT-FFR2, consistent with moderate test–retest reliability.

Discussion

This real-world cohort study evaluated two domestically developed CT-FFR software packages, CFD-driven RuiXin-FFR and deep learning-driven Dr. Wise FFR, together with μQFR for detecting coronary functional ischemia in moderate-to-severe coronary stenosis. Three principal observations were obtained. First, μQFR provided the strongest overall diagnostic performance for coronary functional ischemia, with an AUC of 0.81, an accuracy of 80.39%, and relatively balanced sensitivity and specificity. Second, the two domestically developed CT-FFR software packages demonstrated similar overall diagnostic performance, with AUC values of approximately 0.73 for both, but differed in their diagnostic profiles, particularly with respect to sensitivity/negative predictive value and specificity/positive predictive value. Third, each imaging-derived coronary functional assessment method showed a moderate positive correlation with invasive FFR. Bland–Altman analysis also indicated moderate agreement with invasive FFR, although the LoA remained relatively wide.

Multiple clinical investigations have validated QFR's diagnostic capability for coronary artery functional assessment. The FAVOR Pilot study[18] evaluated fixed-flow QFR (fQFR), contrast-flow QFR (cQFR), and adenosine-flow QFR (aQFR) against invasive FFR to assess functional ischemia in coronary lesions. All three QFR approaches demonstrated favorable agreement with invasive FFR and good diagnostic performance for myocardial ischemia, with accuracies of 80%, 86%, and 87% for fQFR, cQFR, and aQFR, respectively. The subsequent FAVOR II China study[19] reported that QFR outperformed quantitative coronary angiography in both sensitivity and specificity for detecting hemodynamically significant stenosis (94.6% vs. 62.5% and 91.7% vs. 58.1%, respectively), achieving a vessel-level diagnostic accuracy of 93.3%. Consistent diagnostic performance was also observed in the large-scale FAVOR II E/J study[20], in which QFR achieved an accuracy of 86.3%, a specificity of 86.9%, a sensitivity of 86.5%, and an AUC of 0.92 for the functional evaluation of coronary lesions.

Similar favorable outcomes for CT-QFR and μQFR have been documented in comparative studies assessing CT-FFR and μQFR diagnostic performance, including those by Wu et al. and Li et al. Wu et al. [21]reported vessel-level AUC values that were nearly equivalent between CT-QFR and μQFR (0.95 [95%CI, 0.93–0.97] vs. 0.95 [95%CI, 0.92–0.98]). For CT-QFR, the accuracy, sensitivity, specificity, positive predictive value, and negative predictive value for identifying functional ischemia were 92%, 91%, 92%, 83%, and 96%, respectively. The corresponding values for μQFR were 94%, 90%, 97%, 92%, and 96%, respectively. Compared with μQFR, CT-QFR had lower diagnostic accuracy, specificity, and positive predictive value. Both CT-QFR and μQFR showed significant correlations with FFR, with Pearson correlation coefficients of 0.88 and 0.89, respectively. Bland–Altman analysis further indicated a slight underestimation of FFR by CT-QFR (mean bias, 0.003; 95%LoA, − 0.079–0.085).

Li et al. [22]reported that the correlation between CT-QFR and FFR was slightly lower than that observed between μQFR and FFR (r = 0.87 vs. 0.90). Bland–Altman analysis revealed a comparable pattern in the LoA with FFR, with standard deviations of the differences of 0.05 and 0.04, respectively (*P* = 0.064). At the vessel level, CT-QFR also had lower diagnostic accuracy than μQFR (89% vs. 93%; *P* = 0.088). For identifying functional ischemia, the sensitivity, specificity, positive predictive value, and negative predictive value of CT-QFR were 90%, 88%, 85%, and 92%, respectively, compared with 91%, 95%, 93%, and 94% for μQFR. In this study, μQFR demonstrated higher accuracy, specificity, and positive predictive value than the other two CT-FFR methods and also yielded a numerically greater AUC. Nevertheless, statistical significance was not reached for any pairwise comparison among the three methods, possibly attributable to the restricted sample size and consequently limited statistical power. In line with observations by Wu et al. and Li et al., μQFR demonstrated capability in evaluating the hemodynamic relevance of moderate-to-severe coronary stenosis and might offer functional insights to guide revascularization decision-making in high-risk patients who underwent ICA.

In this study, the two domestically developed CT-FFR software packages, RuiXin-FFR based on CFD and Dr. Wise FFR based on a deep learning model, showed comparable overall diagnostic performance for identifying coronary ischemia, with identical AUCs of 0.73 (95%CI, 0.58–0.88) and 0.73 (95%CI, 0.60–0.87), respectively. However, their diagnostic profiles differed. CFD-based RuiXin-FFR had higher sensitivity and negative predictive value, whereas deep learning-based Dr. Wise FFR achieved higher specificity and positive predictive value. Several international head-to-head studies comparing CFD-based and deep learning-based CT-FFR have reported similar overall diagnostic performance between the two approaches, accompanied by differences in sensitivity and specificity[23–25]. Previous studies indicate that CFD-based CT-FFR is derived from three-dimensional coronary artery reconstruction and numerical solution of the Navier–Stokes equations to simulate patient-specific hemodynamics. This method can capture hemodynamic disturbances associated with stenotic and bifurcation lesions and may be less likely to overlook hemodynamically significant lesions. However, its performance depends heavily on accurate vessel segmentation. Calcification or motion artifacts can distort luminal contours, potentially exaggerating trans-stenotic pressure loss and increasing false-positive findings, thereby reducing specificity. In contrast, deep learning-based CT-FFR estimates FFR without directly solving fluid equations by learning the connection between coronary anatomical features and FFR values from large

datasets. This approach may provide greater stability in evaluating ordinary single-vessel stenosis and may generate fewer false-positive results. However, when heavily calcified, serial, or complex bifurcation lesions are insufficiently represented in the training data, model generalizability may decline, increasing the likelihood that ischemic lesions are missed [26].

Correlation and agreement analyses indicated only moderate positive associations between the two CT-FFR software packages and invasive FFR (r = 0.411, *P* = 0.003; r = 0.438, *P* = 0.001), while Bland–Altman analysis displayed relatively wide LoA. This pattern was generally consistent with findings from other real-world retrospective cohort studies[27]. Unlike prospective multicenter trials that typically apply stringent eligibility criteria and include images of optimal quality, real-world cohorts more frequently involve calcified lesions, arrhythmias, and image noise, all of which may reduce agreement between CT-FFR and invasive FFR. In this study, RuiXin-FFR tended to underestimate FFR systematically, with a mean bias of 0.064, whereas Dr. Wise FFR showed a smaller mean bias of 0.020 and values closer to invasive FFR. Similar bias patterns have been described in previous software validation studies[28]. CFD simulation often applies standardized and simplified assumptions to microcirculatory boundary conditions, which may introduce directional measurement bias. By contrast, deep learning models can learn and adjust for systematic errors during training on large datasets, potentially resulting in lower overall measurement bias.

A meta-analysis reported that the sensitivity and specificity of CT-FFR for ischemia detection generally ranged from 63% to 100% and from 52% to 98%, respectively, with diagnostic variability closely associated with lesion characteristics and image quality across study populations[29]. This study used a retrospective cohort design within routine clinical practice and reflects real-world clinical conditions to some extent. Nevertheless, selection bias may remain because of suboptimal image quality and complex lesion characteristics, and the external generalizability of these findings requires additional validation. The Expert Consensus states that CT-FFR, whether based on CFD or deep learning approaches, cannot completely substitute for invasive FFR and that functional results should be interpreted together with calcification burden, lesion anatomy, and clinical symptoms[1].

Based on prior evidence and the present results, CT-FFR1 (RuiXin-FFR) exhibited relatively high sensitivity and negative predictive value, suggesting potential utility for excluding functional ischemia. However, its role in clinical triage requires confirmation in larger prospective cohorts of patients with chest pain. CT-FFR2 (Dr. Wise FFR) showed a tendency toward higher specificity and may offer supplementary functional information for patients being considered for interventional treatment. Direct comparisons between domestically developed CFD-based and deep learning-based CT-FFR software remain scarce, while most comparable international studies have evaluated imported algorithms and provide limited guidance for the clinical use of domestic devices. This study adds real-world comparative evidence for these two domestically developed CT-FFR tools. Larger studies incorporating subgroup analyses are needed to characterize algorithm-specific performance in heavily calcified, bifurcation, and serial stenotic lesions and to define more precisely the patient populations and lesion subtypes most suitable for domestically developed CT-FFR software.

Notwithstanding these encouraging results, this work has inherent limitations that need to be considered when interpreting our data. First, the retrospective single-center design and relatively small sample size limited the robustness of this study. Given that inclusion was confined to vessels from patients who had undergone CCTA, ICA, and FFR measurement, selection bias may have occurred. These factors restrict the generalizability of the findings and warrant cautious interpretation. These findings warrant confirmation via larger multicenter, prospective investigations.

Second, severe stenosis was overrepresented in the study population, with lesions showing 70%–90% stenosis accounting for 74.51% and those with 50%–69% stenosis accounting for 25.49%. Moderate-to-severe lesions frequently present with complex anatomical characteristics, including calcification, tortuosity, bifurcations, and multivessel involvement. These features may reduce the accuracy of imaging-derived coronary functional assessment methods, particularly in bifurcation, diffuse, and serial lesions. In the FFR gray zone and in acute myocardial infarction, these anatomical complexities may influence computational assumptions and impair diagnostic performance[30].

Third, the findings may also have been influenced by operator experience and the level of workflow standardization. Interobserver agreement was good in this study (ICC > 0.85), whereas repeated measurements by the same observer yielded an ICC of 0.65, indicating only moderate intraobserver reproducibility for both CT-FFR methods. Variability in coronary segmentation boundaries, manual correction procedures, and measurement-site selection may partly explain this finding. Therefore, despite the use of automated analysis software, manual interaction may still influence result stability.

Fourth, target lesion locations in the CT-FFR and μQFR analyses were individually matched to those assessed by invasive FFR. However, the measurement sites for CT-FFR and μQFR were not identical because of method-specific measurement standards. CT-FFR was measured 2 cm distal to the target lesion, whereas μQFR was obtained at the distal end of the target vessel. This difference in measurement location may have influenced the comparison between the two methods.

Conclusions

Among patients who underwent CCTA, ICA, and invasive FFR, all three imaging-derived functional assessment methods demonstrated the ability to identify functional ischemia in moderate-to-severe coronary lesions (50%–90%). μQFR achieved the highest AUC and accuracy, while maintaining relatively balanced sensitivity and specificity. The two domestically developed CT-FFR software showed similar overall diagnostic performance but differed across individual diagnostic indices. Because of the limited sample size and overlapping AUC confidence intervals, these findings should be interpreted as indicating potential differences in performance rather than definitive superiority of any method. Larger multicenter prospective studies are required for further validation.

Abbreviations

AUC

Area under the receiver operating characteristic curve CAD:Coronary artery disease CAD-RADS:Coronary Artery Disease Reporting and Data System CCTA:Coronary computed tomography angiography CFD:Computational fluid dynamics CI:Confidence interval CT-FFR:Computed tomography angiography-derived fractional flow reserve FFR:Fractional flow reserve HU:Hounsfield units ICA:Invasive coronary angiography ICC:Intraclass correlation coefficient IQR:Interquartile range LAD:Left anterior descending artery LCX:Left circumflex artery LoA:Limits of agreement NPV:Negative predictive value PPV:Positive predictive value QFR:Quantitative flow ratio RCA:Right coronary artery ROC:Receiver operating characteristic SD:Standard deviation μQFR:Murray law-based quantitative flow ratio

Declarations

Ethics approval and consent to participate

The study complied with the Declaration of Helsinki of the World Medical Association and all applicable regulations. Because the analysis used retrospective data, written informed consent was waived in accordance with relevant regulatory provisions. Ethical approval was granted by the Medical Ethics Committee of the Affiliated LiHuiLi Hospital of Ningbo University(Approval No.: KY2024SL057-03; Approval Date: 13 January 2026).

Consent for publication

Not applicable.

Competing interests

The authors report no competing interests.

Authors’ information

Not applicable.

Funding

Not applicable.

Author Contribution

Z conceived and designed the study. H, W and X collected the data. X performed the statistical analysis. H drafted the manuscript. All authors reviewed and approved the final manuscript.

Acknowledgements

Not applicable.

Availability of data and materials

The datasets supporting this study's conclusions are obtainable from the corresponding author upon a reasonable request.

References

1. Chinese Society of Cardiology. Chin Med Association □□□□CT□□□□□□□□□□□□□□□□□□□□ □□□□□□□□□□□. 2023;31:241–51.
2. Achenbach S, Rudolph T, Rieber J, Eggebrecht H, Richardt G, Schmitz T, et al. Performing and interpreting fractional flow reserve measurements in clinical practice: an expert consensus document. Interv Cardiol Rev. 2017;12:97. 10.15420/icr.2017:13:2.
3. Demir OM, Schrieken C, Curio J, Rahman H. Behavioural determinants impacting the adoption rate of coronary physiology. Int J Cardiol. 2021;330:12–4. 10.1016/j.ijcard.2021.02.008.
4. Song L, Xu B, Tu S, Guan C, Jin Z, Yu B, et al. 2-year outcomes of angiographic quantitative flow ratio-guided coronary interventions. J Am Coll Cardiol. 2022;80:2089–101. 10.1016/j.jacc.2022.09.007.
5. Koo B-K, Erglis A, Doh J-H, Daniels DV, Jegere S, Kim H-S, et al. Diagnosis of ischemia-causing coronary stenoses by noninvasive fractional flow reserve computed from coronary computed tomographic angiograms. J Am Coll Cardiol. 2011;58:1989–97. 10.1016/j.jacc.2011.06.066.
6. Bennar W, Arroyo D, Oppé C, Garin D, Allemann L, Pittet T, et al. Diagnostic accuracy of angiography-derived Murray law-based quantitative flow ratio (μQFR) versus pressure-derived fractional flow reserve (FFR) in moderate to severe calcified coronary lesions—the DIAMOND study. Cathet Cardio Intervent. 2025;106:377–83. 10.1002/ccd.31553.
7. Li G, Weng T, Sun P, Li Z, Ding D, Guan S, et al. Diagnostic performance of fully automatic coronary CT angiography-based quantitative flow ratio. J Cardiovasc Comput Tomogr. 2025;19:40–7. 10.1016/j.jcct.2024.10.001.
8. Hwang D, Park S-H, Nam C-W, Doh J-H, Kim HK, Kim Y, et al. Diagnostic performance of on-site automatic coronary computed tomography angiography-derived fractional flow reserve. Korean Circ J. 2024;54:382. 10.4070/kcj.2023.0288.
9. Han W, Liang L, Han T, Wang Z, Shi L, Li Y, et al. Diagnostic performance of the quantitative flow ratio and CT-FFR for coronary lesion-specific ischemia. Sci Rep. 2024;14:16969. 10.1038/s41598-024-68212-1.
10. Tanigaki T, Emori H, Kawase Y, Kubo T, Omori H, Shiono Y, et al. QFR versus FFR derived from computed tomography for functional assessment of coronary artery stenosis. JACC Cardiovasc

Interv. 2019;12:2050–9. 10.1016/j.jcin.2019.06.043.

11. Cury RC, Leipsic J, Abbara S, Achenbach S, Berman D, Bittencourt M, et al. CAD-RADS 2.0–2022 coronary artery disease-reporting and data system. J Cardiovasc Comput Tomogr. 2022;16:536–57. 10.1016/j.jcct.2022.07.002.
12. Abbara S, Arbab-Zadeh A, Callister TQ, Desai MY, Mamuya W, Thomson L, et al. SCCT guidelines for performance of coronary computed tomographic angiography: a report of the Society of Cardiovascular Computed Tomography Guidelines Committee. J Cardiovasc Comput Tomogr. 2009;3:190–204. 10.1016/j.jcct.2009.03.004.
13. Chinese Society of Cardiology, Chinese Medical Association. [illegible]. (2025). [illegible]. 2025;53:717. 10.3760/cma.j.cn112148-20250422-00302
14. Chinese Society of Cardiology, Chinese Medical Association. [illegible]. 2025;53:460. 10.3760/cma.j.cn112148-20240515-00267.
15. Chen YC, Zhou F, Wang YN, Zhang JY, Yu MM, Hou Y, et al. Optimal measurement sites of coronary-computed tomography angiography-derived fractional flow reserve: the insight from China CT-FFR study. J Thorac Imaging. 2023;38:194–202. 10.1097/RTI.0000000000000687.
16. Cai Z, Yu T, Yang Z, Hu H, Lin Y, Zhang H, et al. Detecting lesion-specific ischemia in patients with coronary artery disease with computed tomography fractional flow reserve measured at different sites. BMC Med Imaging. 2023;23:76. 10.1186/s12880-023-01031-4.
17. Huang W, Liu Y, Wang Q, Jin H, Tang Y, Wang J, et al. Diagnostic performance of target vs. vessel μFR in stable coronary artery disease. BMC Cardiovasc Disord. 2025;25:345. 10.1186/s12872-025-04757-x.
18. Tu S, Westra J, Yang J, von Birgelen C, Ferrara A, Pellicano M, et al. Diagnostic accuracy of fast computational approaches to derive fractional flow reserve from diagnostic coronary angiography. JACC Cardiovasc Interv. 2016;9:2024–35. 10.1016/j.jcin.2016.07.013.
19. Xu B, Tu S, Qiao S, Qu X, Chen Y, Yang J, et al. Diagnostic accuracy of angiography-based quantitative flow ratio measurements for online assessment of coronary stenosis. J Am Coll Cardiol. 2017;70:3077–87. 10.1016/j.jacc.2017.10.035.
20. Westra J, Andersen BK, Campo G, Matsuo H, Koltowski L, Eftekhari A, et al. Diagnostic performance of in-procedure angiography-derived quantitative flow reserve compared to pressure-derived fractional flow reserve: the FAVOR II Europe-Japan study. J Am Heart Assoc. 2018;7:e009603. 10.1161/JAHA.118.009603.
21. Wu X, Wang K, Li G, Wu J, Jiang J, Gao F, et al. Diagnostic performance of angiography-derived quantitative flow ratio in complex coronary lesions. Circ Cardiovasc Imaging. 2024;17:e016046. 10.1161/CIRCIMAGING.123.016046.
22. Li Z, Li G, Chen L, Ding D, Chen Y, Zhang J, et al. Comparison of coronary CT angiography-based and invasive coronary angiography-based quantitative flow ratio for functional assessment of coronary stenosis: a multicenter retrospective analysis. J Cardiovasc Comput Tomogr. 2022;16:509–16. 10.1016/j.jcct.2022.06.002.

23. Narimani-Javid R, Moradi M, Mahalleh M, Najafi-vosough R, Arzhangzadeh A, Khalique O, et al. Machine learning and computational fluid dynamics derived FFRCT demonstrate comparable diagnostic performance in patients with coronary artery disease: a systematic review and meta-analysis. J Cardiovasc Comput Tomogr. 2025;19:232–46. 10.1016/j.jcct.2025.02.004.
24. Coenen A, Kim Y-H, Kruk M, Tesche C, De Geer J, Kurata A, et al. Diagnostic accuracy of a machine-learning approach to coronary computed tomographic angiography-based fractional flow reserve: result from the MACHINE consortium. Circ Cardiovasc Imaging. 2018;11:e007217. 10.1161/CIRCIMAGING.117.007217.
25. Tesche C, De Cecco CN, Baumann S, Renker M, McLaurin TW, Duguay TM, et al. Coronary CT angiography-derived fractional flow reserve: machine learning algorithm versus computational fluid dynamics modeling. Radiology. 2018;288:64–72. 10.1148/radiol.2018171291.
26. Peters B, Paul J-F, Symons R, Franssen WMA, Nchimi A, Ghekiere O. Invasive fractional-flow-reserve prediction by coronary CT angiography using artificial intelligence vs. computational fluid dynamics software in intermediate-grade stenosis. Int J Cardiovasc Imaging. 2024;40:1875–80. 10.1007/s10554-024-03173-0.
27. Gaur S, Øvrehus KA, Dey D, Leipsic J, Bøtker HE, Jensen JM, et al. Coronary plaque quantification and fractional flow reserve by coronary computed tomography angiography identify ischaemia-causing lesions. Eur Heart J. 2016;37:1220–7. 10.1093/eurheartj/ehv690.
28. Zhou B, Guo Y, Guo D, Qian S, Huang Z, Zhang Y, et al. Comparative diagnostic performance and stability of deep learning- and CFD-based CT-FFR across vessels, cardiac phases, and centers. Front Cardiovasc Med. 2026;13:1883012. 10.3389/fcvm.2026.1883012.
29. Zhuang B, Wang S, Zhao S, Lu M. Computed tomography angiography-derived fractional flow reserve (CT-FFR) for the detection of myocardial ischemia with invasive fractional flow reserve as reference: systematic review and meta-analysis. Eur Radiol. 2020;30:712–25. 10.1007/s00330-019-06470-8.
30. Lee KY, Hwang B-H, Kim MJ, Choo E-H, Choi IJ, Kim CJ, et al. Influence of lesion and disease subsets on the diagnostic performance of the quantitative flow ratio in real-world patients. Sci Rep. 2021;11:2995. 10.1038/s41598-021-82235-y.

Figures

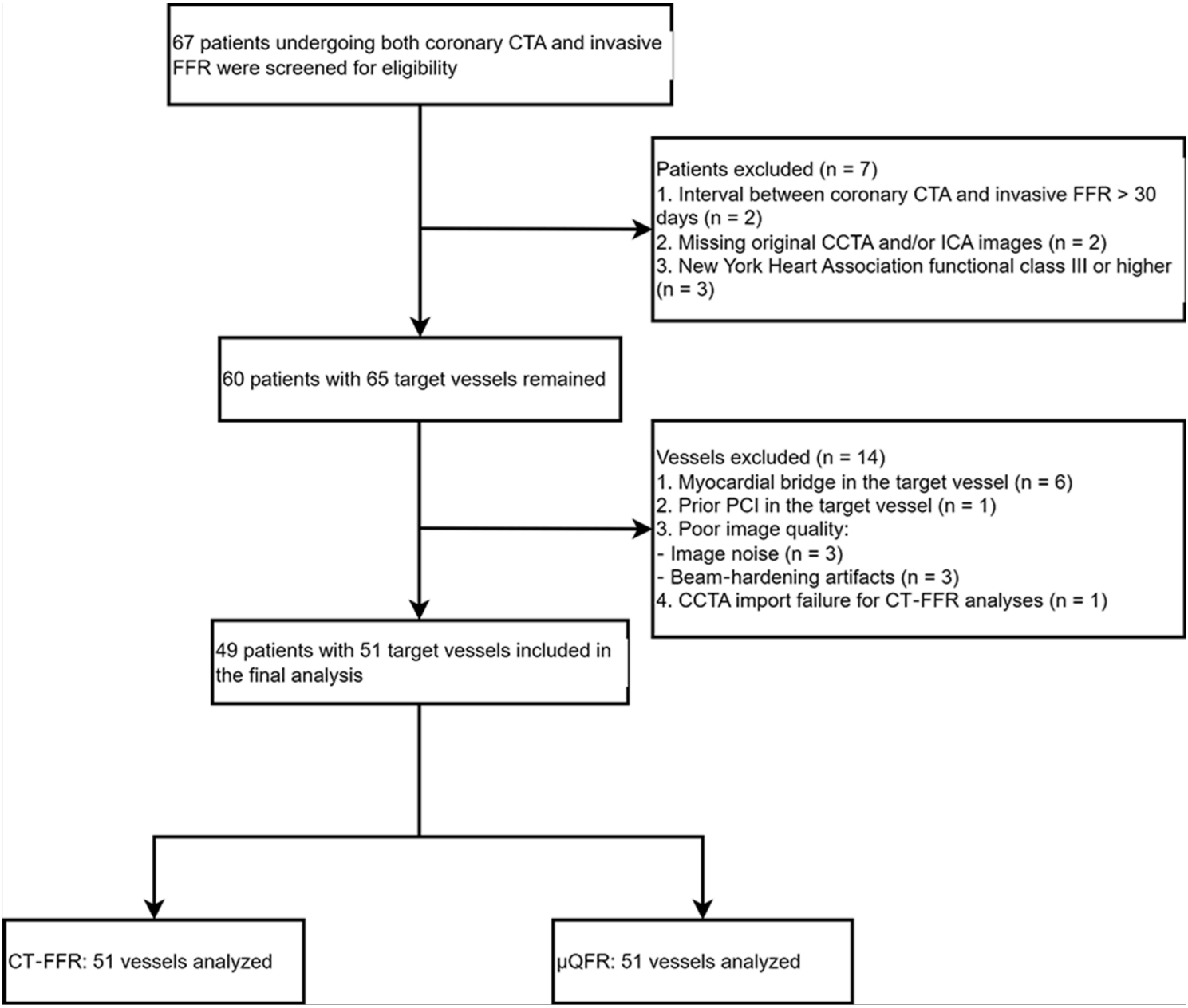


Figure 1

Flow chart of enrollment.

n denotes the number of vessels. CCTA, coronary computed tomography angiography; ICA, invasive coronary angiography; FFR, fractional flow reserve; CT-FFR, quantitative flow ratio derived from computed tomography angiography; μQFR indicates Murray law–based quantitative flow ratio; PCI, percutaneous coronary intervention.

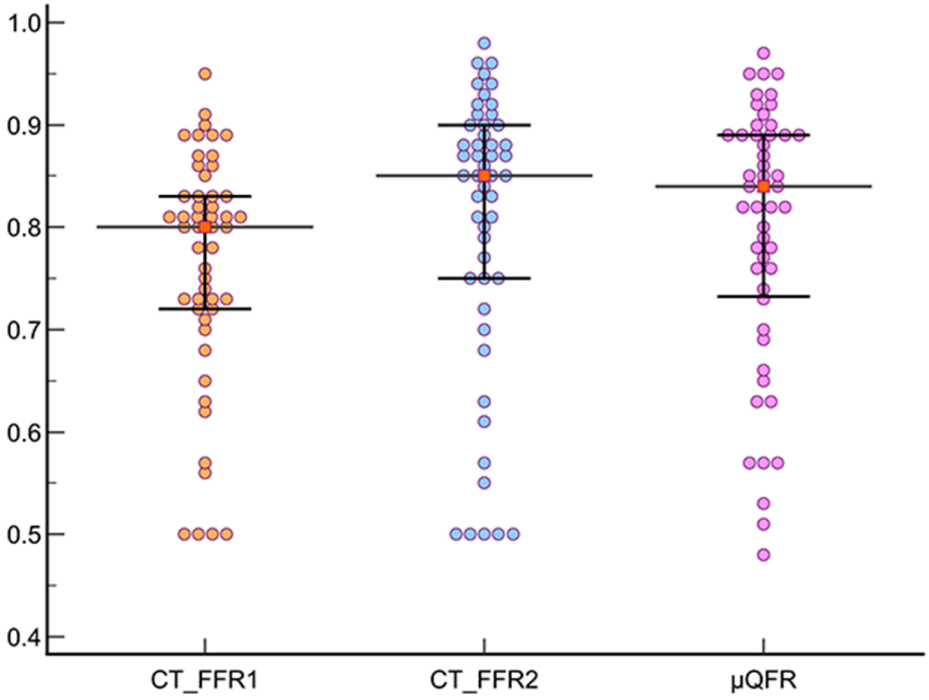


Figure 2

Distribution of CT-FFR1, CT-FFR2, and μQFR.

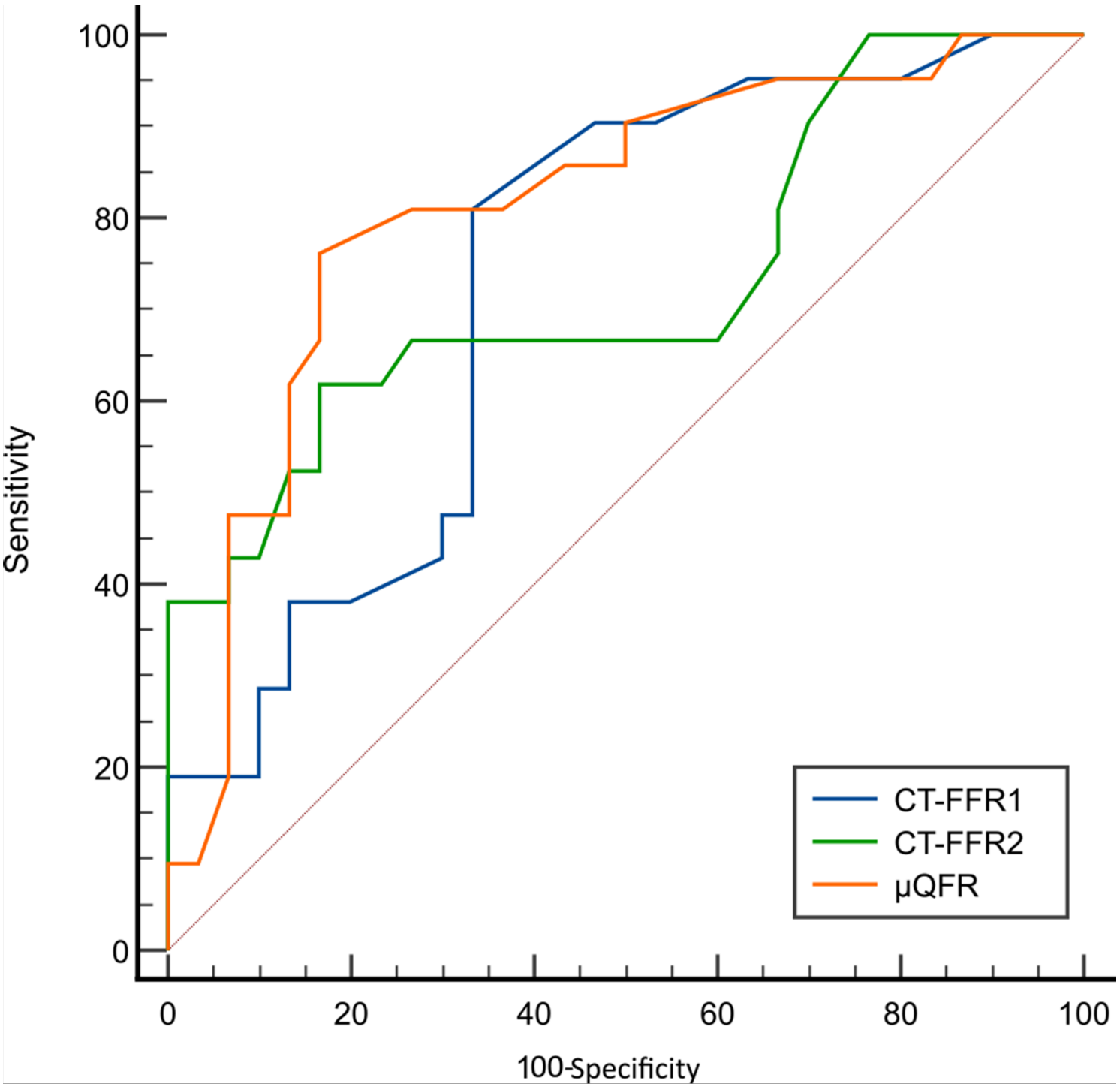


Figure 3

ROC curves of CT-FFR1, CT-FFR2 and μQFR for detection of functionally significant coronary stenosis, with invasive FFR as the reference.

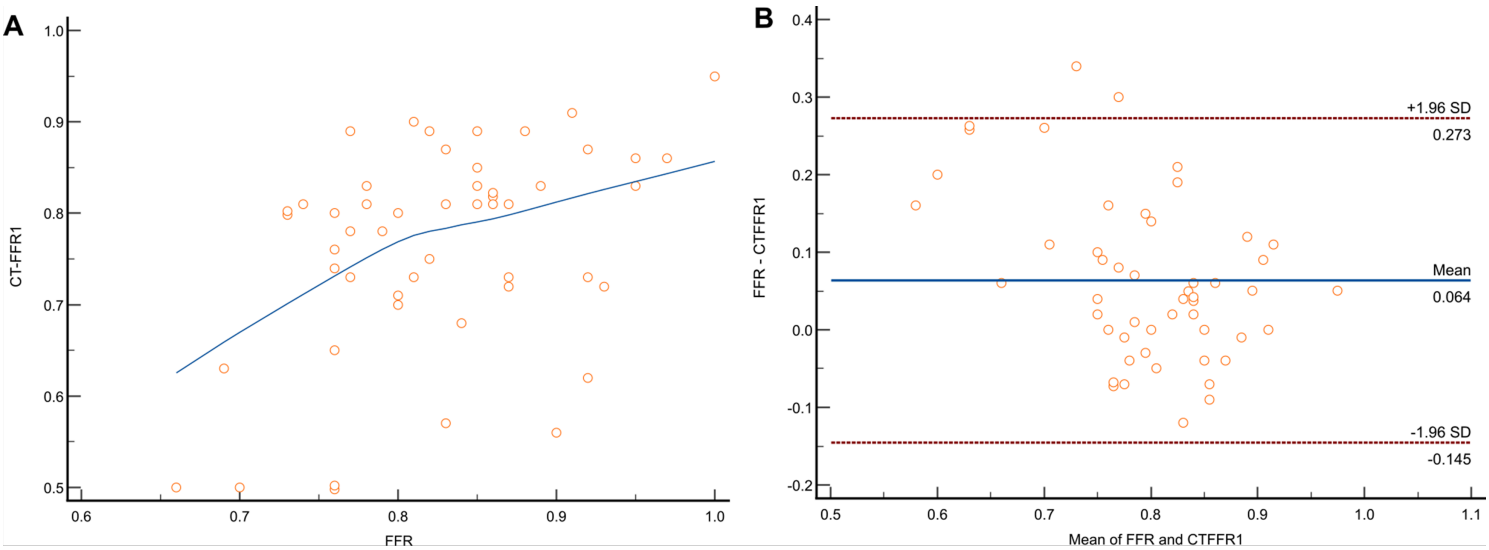


Figure 4

Correlation (A) and Bland-Altman (B) plots of invasive FFR versus CT-FFR1. Solid blue line = mean difference; red dashed lines = 95% limits of agreement.

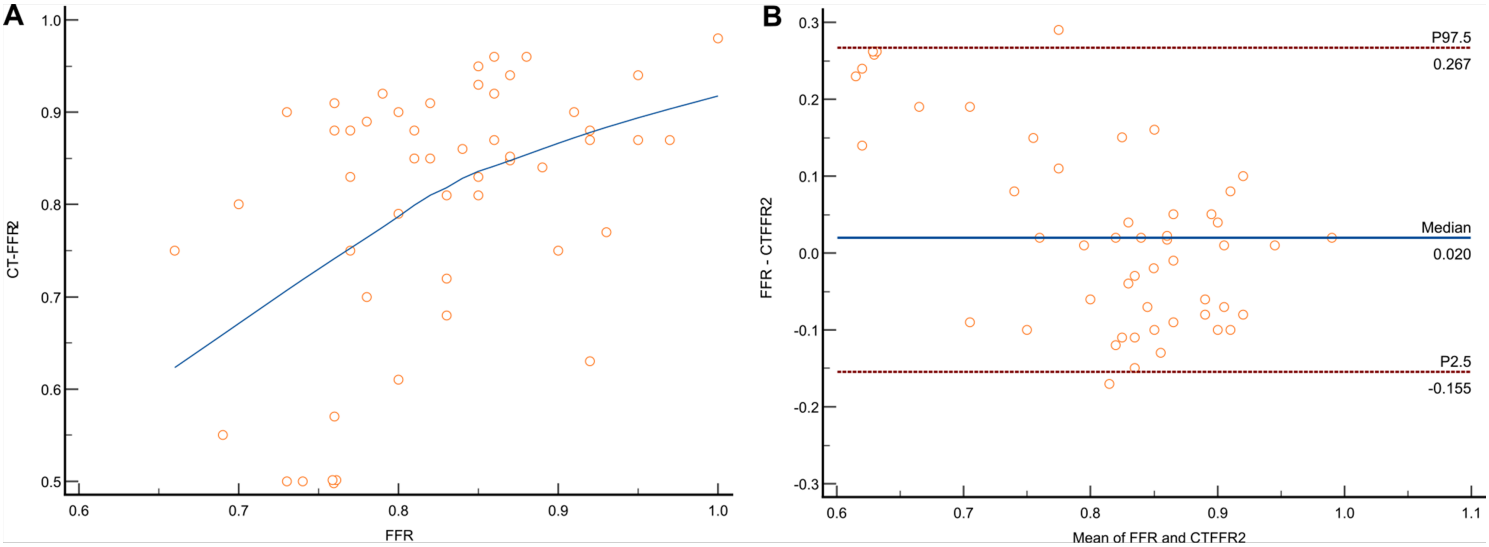


Figure 5

Correlation (A) and Bland-Altman (B) plots of invasive FFR versus CT-FFR2. Solid blue line = median difference; red dashed lines = 2.5th and 97.5th percentiles.

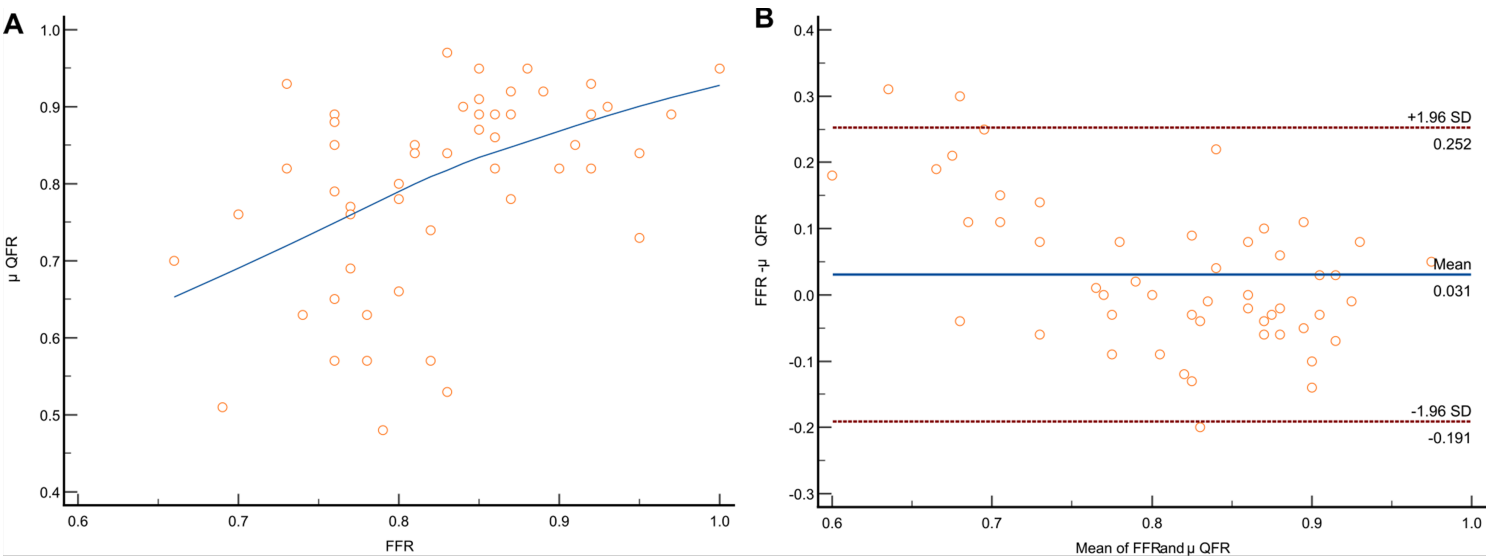


Figure 6

Correlation (A) and Bland-Altman (B) plots of invasive FFR versus μQFR. Solid blue line = mean difference; red dashed lines = 95% limits of agreement.